

Design and Test of a Planarized High Power Density 100 kW SiC Traction Inverter with 1kV DC-Link

Li Yang, Yukun Luo, Radha Sree Krishna Moorthy, Dhruvo Rahman, Wensong Yu, Iqbal Husain
FREEDM System Center
North Carolina State University
Email: {lyang20,yluo9,rkrish12,drahman,wyu2,ihusain2}@ncsu.edu

Abstract—A SiC MOSFET based 1kV DC-link planarized traction inverter is designed to achieve high power density and high common mode noise immunity of the gate driver. To achieve high power density, a planarized structure is adopted to reduce the overall height of the whole system. Significantly, PCB based busbar, gate driver planar transformer and shunt-based current sensor are the main concepts for planarized inverter design. Moreover, a split gate driver concept is used to shrink the overall size of inverter and reduce driving loop inductance as well. An optimized planar transformer winding layout has been used to reduce the coupling capacitance between primary and secondary side in order to achieve high common mode noise immunity. The inverter is designed for 100kW continuous power and has been tested with a novel closed-loop high power circulating strategy that requires only a small rating DC power supply. Testing results verify the design concepts and the high performance of the traction inverter.

Index Terms—SiC MOSFET, traction inverter, low profile, high common mode transient immunity(CMTI), high power density.

I. INTRODUCTION

Silicon Carbide(SiC) MOSFET as a wide bandgap device provides a lot of merits that are especially favored by electrical vehicle (EV) industry. Compared with Si IGBT, SiC device has lower switching and conduction losses that is important for EV mileage extension. The high junction temperature operation capability makes it possible to design integrated powertrain with reduced cooling requirement. High switching frequency of the SiC device reduces size of passive components in the powertrain system including DC-link capacitor, boost inductor and EMI filter. Because of the features of SiC device, overall size of the powertrain can be reduced, which makes SiC device a good candidate to achieve high power density for EV powertrain.

High power density design, among high temperature operation and high efficiency operation, has been one of the main focus of researches on SiC traction inverter. A 35kW SiC traction inverter is designed in [1] with power density of 70kW/L. The SiC module is designed with Schottky Barrier Diode(SBD) removed, which reduces switching loss and the size of heat sink. In [2] and [3], 50kW traction inverters are designed with SiC JFET and SiC MOSFET, respectively. Both of the designs have gate assistant circuit to achieve fast switching of SiC device. The power density achieved

by the works are 8.5kW/kg and 26kW/kg, respectively. The work in [4] reports a liquid-cooled 55kW traction inverter designed with front-end boost stage, the inverter is designed with four six-pack SiC MOSFETs and features a planarized structure, overall power density achieved is 12.1kW/L. In [5], Fraunhofer developed liquid cooled 60kW SiC inverter for high speed drives. The design uses a high DC-link voltage (900V_{dc}) and power module with integrated gate driver that can switch at 100kHz with low loss. The achieved power density is 160kW/L. Mitsubishi developed HEV powertrain with both motor/generator inverter and front-end boost stage at a total power level of 430kVA[6]. The power module is designed to have low commutation loop inductance that enables fast switching, direct soldering of the module on heat sink improves the thermal conductivity. Achieved power density of the design is 86kVA/L. In [7], Wolfspeed developed 250kW traction inverter using off-the-shelf low profile low inductance full SiC module. The inverter is reported to operate under 150°C ambient temperature and achieves power density of 15.6kW/kg.

Recently, high DC-link voltage traction inverter has been introduced to EV powertrain design. While the majority passenger electrical vehicle manufactures now adopts 400V system for the traction inverter, which has a DC-link voltage of 150V-450V, an 800V system which has DC-link of up to 870V has come into market and provides benefits to the EV powertrain[8][9]. Compared with 800V system, the 400V system needs to operate with much higher phase current that increases temperature and loss of the busbar and power cable. Moreover, high current operation also reduces reliability of the DC-link capacitors. As analyzed in [10], the DC-link ripple current directly relates with the magnitude of AC current output. Therefore, DC-link capacitor of the high current inverter needs to sink and source high ripple current, which is usually achieved by paralleling more capacitor cells at the sacrifice of power density and cost.

In this paper, the design optimizations on the busbar, gate driver and current sensor are discussed. The paper presents a planarization design method that can achieve high power density of the inverter as shown in Fig. 1. The inverter is designed for 100kW continuous power with 1kV DC-link to investigate both the benefits and issues of high DC-link

traction inverter as discussed in [8]. At last, a high power circulating test strategy is used to test the inverter up to 100kW without the need of high rating DC power supplies and load banks.

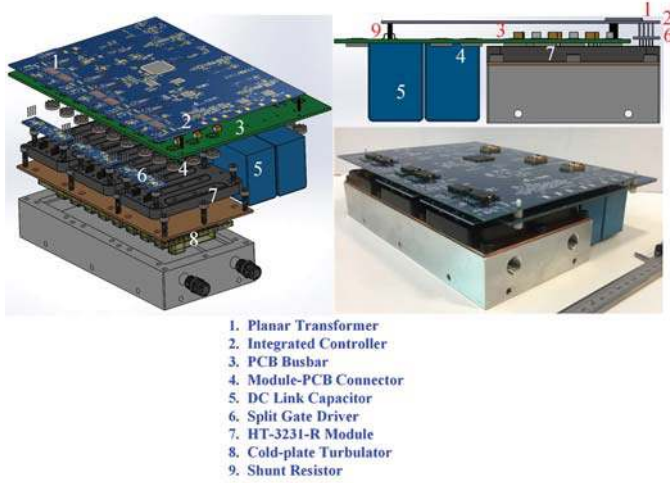


Fig. 1: Assembly view of the planar structure.

II. PCB BUSBAR DESIGN FOR 1.7 kV SiC MODULE

The 1kV DC-link design is achieved using Wolfspeed's state-of-the-art 1.7kV/8mΩ full SiC MOSFET module HT-3231. The module shares the same high performance 62mm half-bridge package as Wolfspeed's off-the-shelf 1.2kV/3.7mΩ module CAS325M12HM2. A detailed ANSYS Q3D modeling and parasitic inductance simulation has been conducted for the used module in [11], module inductance from DC+ to DC- is 10.48nH at 10MHz. The modeling of the 1.2kV/3.7mΩ module is shown in Fig.2.

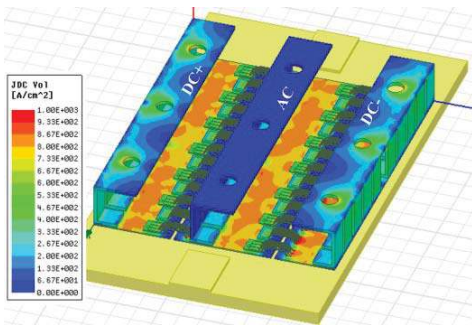


Fig. 2: Modeling of off-the-shelf 1.2kV/3.7mΩ module in ANSYS Q3D.

A. Characteristic Impedance Minimization

As the interconnection of power components of the inverter, a low characteristic impedance of busbar is critical to attenuate high frequency noise and EMI. Characteristic impedance is expressed by (1):

$$Z = \sqrt{\frac{L}{C}} = \sqrt{\frac{L_p + L_n - 2L_m}{C_{dd}}} \quad (1)$$

where L_p and L_n are the self-inductance of DC+ and DC- planes of the busbar, L_m is the mutual-inductance and C_{dd} is the coupling capacitance of the planes. Modeling DC planes of the busbar as two parallel copper sheets with the geometries shown in Fig.3, the parasitic parameters of the busbar can be calculated by (2).

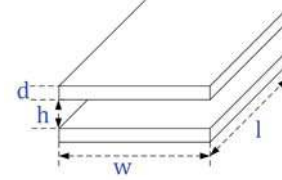


Fig. 3: Modeling busbar by parallel copper sheets.

$$L_{p,n} = \frac{\mu_0 \mu_r l}{\pi} \left(\frac{1}{8} + \frac{2d}{d+w} \right) \quad (h \ll w, d \ll w)$$

$$L_m = \frac{\mu_0 \mu_r l \cdot d}{\pi \sqrt{4(d+h)^2 + kW^2}} \cos \theta \quad (2)$$

$$C_{dd} = \epsilon_0 \epsilon_r \frac{w \cdot l}{h}$$

where μ_0 , μ_r are the vacuum permeability and the relative permeability of the insulating material, ϵ_0 , ϵ_r are electric constant and relative static permittivity of the insulating material and θ the angle between the planes[12]. According to (2), $L_{p,n}$ can be minimized by decreasing l and d while increasing w . L_m can be maximized by increasing l and d while decreasing h . C_{dd} can be maximized by increasing l and w while decreasing h . There are trade-offs to be made on l and d , but the width w and distance h of the DC copper planes needs to be maximized and minimized, respectively, to reduce the characteristic impedance. The designed PCB busbar uses 4oz. copper each layer to provide enough current conduction capability and increase L_m , the busbar is designed for 8 layers with the stack shown in Fig.4. By placing DC planes adjacently, h is reduced and L_m , C_{dd} are increased. By designing two sets of DC planes, the current conduction capability of the busbar is increased as well as the C_{dd} .

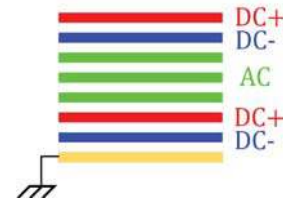


Fig. 4: Layer stack of the designed PCB busbar.

A chassis ground layer is also added for the PCB busbar that has two benefits: (1)the chassis ground helps to reduce the commutation loop inductance. The result has been verified by ANSYS Q3D simulation for the busbar with and without the chassis ground; (2)the chassis ground forms Y capacitor with both the AC and DC planes, which helps attenuate high

frequency EMI noise from the inverter[13]. As the overlap between DC planes are maximized to increase the stray capacitance, the overlap between the AC planes and DC planes are minimized. The reason is that these planes are essentially the drain and source for the top and bottom switches, so overlapping them will increase the output capacitance C_{oss} . Therefore, switching speed decreased and switching loss increased if the overlap is enlarged. The overlap area for the designed busbar is minimized for current conduction capability of 100A.

B. Commutation Loop Optimization

Commutation loop inductance minimization is critical for the busbar design. Usually, the commutation loop is formed by the DC-link capacitors, the conduction path inside the power module and the stray inductance on the busbar between them. Low ESL DC-link capacitor, optimized busbar layout and high performance module all help to reduce the loop inductance. Adding low ESL decoupling capacitor in close vicinity to the module is another effective method to reduce the loop inductance. The design is shown in Fig.5 where $Loop_1$ is formed by DC-link capacitors and $Loop_2$ is formed by the decoupling capacitors.

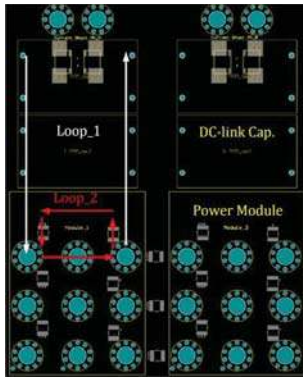


Fig. 5: Layout of commutation loops for two phases on the PCB busbar.

Busbar design adopting a central electrolytic DC-link capacitor can result in unsymmetrical commutation loops for different phases and cause the highest V_{ds} overshoot as well as switching loss for one particular phase. Therefore, the commutation loops for three phase voltage source inverter should be designed as symmetrical as possible especially for high power applications. Also shown in Fig.5, two film DC-link capacitors totally 54uF and six ceramic decoupling capacitors are designed identically for each phase. The total inductance of commutation loop $Loop_2$ is 12.8nH at 10MHz.

C. Overall Design of the Busbar

The PCB based busbar for 100kW SiC traction inverter is designed based on the optimizations and methods discussed above, the top and side view of the busbar are shown in Fig.6(a) and Fig.6(b). The layout of three phase circuits are

identical and totally 162uF DC-link capacitor is designed for the busbar.

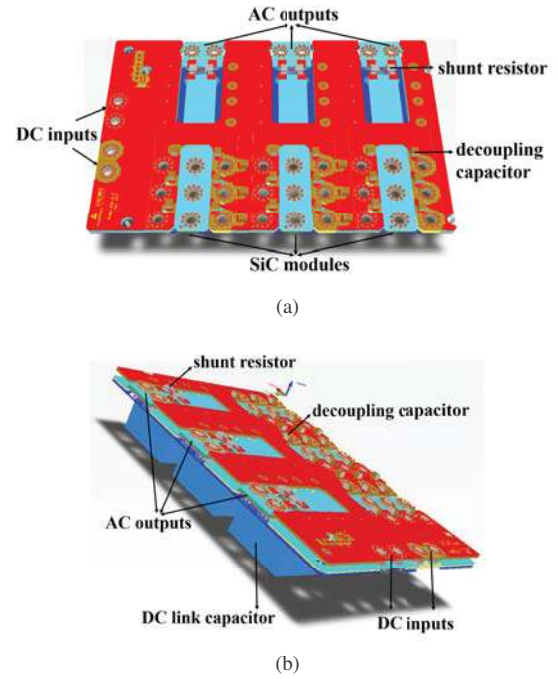


Fig. 6: 3D layout of the PCB busbar (a) top view (b) side view.

III. LOW PROFILE GATE DRIVER

A. Gate Driver Power Supply Architecture

The key concept on optimizing gate driver isolation transformer is by high frequency operation. Increasing transformer operating frequency, smaller core can be used which makes low profile planar transformer possible. High frequency operation also reduces the number of turns needed for the windings, which reduces the coupling capacitance between the windings as a result.

To achieve high frequency operation, a transformer driver MAX13256 from Maxim is selected. Architecture of the designed gate driver power supply is shown in Fig.7 following [14]. The transformer driver converts 24V DC to $\pm 24V$ square wave at a frequency around 450kHz. The high frequency AC link is then shared by two planar transformers for the top and bottom driver circuits and rectified to generate +19V/-5V rails.

High frequency core material 3F35 is chosen for low core loss. In [15], a modified core loss density model is proposed for square wave excited transformer and the predicted core loss under square wave excitation is given by:

$$P_{core} = \frac{8}{\pi^2 [4D(1-D)]^{\gamma+1}} K f^\alpha B^\beta \quad (3)$$

where $D=0.5$ is fixed by MAX13256, $\gamma = -0.12$ is the curve fitting coefficient for 3F35 material under 500kHz square wave excitation and $K f^\alpha B^\beta$ is the core loss predicted by Steinmetz equation under sinusoidal excitation, which is given in core

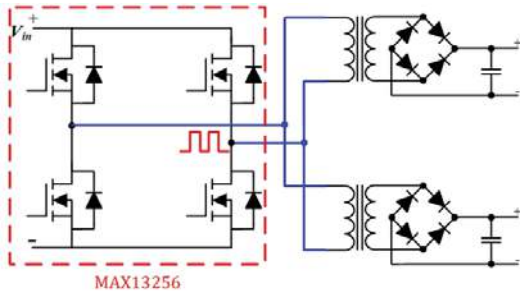


Fig. 7: Architecture of the designed gate driver power supply.

material datasheet. An EI core combination E18/4/10/R-3F35 and PLT18/10/2/S-3F35 from Ferroxcube are chosen for the planar transformer, assuming 0.1W loss on the core, according to

$$\frac{8}{\pi^2[4D(1-D)]^{\gamma+1}} K f^\alpha B^\beta = \frac{0.1 \times 10^{-3}}{V_e}$$

$K f^\alpha B^\beta = 148.6 \text{ kW/m}^3$, where $V_e = 830 \text{ mm}^3$ is the effective core volume of the selected EI core. The corresponding peak flux density can be found to be $\Delta B = 60 \text{ mT}$ from the power loss vs. peak flux density curve of the material. Using (4), the number of turns for the transformer can be calculated, where $v \cdot \Delta t = 26.4 \text{ V} \cdot \mu\text{s}$ is the applied volt-sec and $A_e = 40 \text{ mm}^2$ is the effective core area.

$$N = \frac{v \cdot \Delta t}{2 \cdot A_e \cdot \Delta B} = 5.5 \quad (4)$$

B. Transformer Inter-winding Capacitance Minimization

Isolation transformer with low inter-winding capacitance is critical for SiC device based inverter that operates with high dv/dt . The inter-winding capacitance of transformer consists of two contributors [16]. As shown in Fig.8, the C_{ww} is the winding-winding capacitance formed by primary and secondary windings; the C_{wccw} is the winding-core-winding capacitance formed by the windings and the core. To reduce the inter-winding capacitance, both C_{ww} and C_{wccw} needs to be minimized.

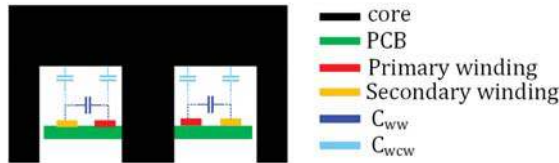


Fig. 8: Two stray capacitance components contributing the total coupling capacitance.

The winding layout is on a six layer PCB. To decide the inter-winding capacitance contributed by C_{ww} , three layouts for N=6, 5, and 4 are first simulated in ANSYS Q3D. As shown in Fig.9, the inner windings are for primary side and the outer windings are for secondary side. For N=6, two turns are designed on each layer, while for N=5 and 4, one turn is on each layer. The simulated inter- and intra-

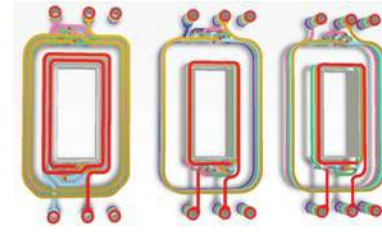


Fig. 9: Layout of the PCB transformer for N=6, 5, 4 from left to right.

winding capacitances are tabulated in Table I. Compare the results for N=6 and N=5,4, a significant reduction on inter-winding capacitance (C_{ww}) is achieved because of the increase on distance between primary and secondary windings. The winding-core-winding capacitance (C_{wccw}) is also expect to reduce, because with less turns on each layer, the overlap area between the windings and core is reduced. Compare the results for N=5 and N=4, there are minor reduction on C_{ww} because the pattern for the two layouts are similar, both the C_{ww} and C_{wccw} will be similar.

TABLE I: Stray capacitance comparison for N=6, 5 and 4.

No. of turns	Intra-winding	Inter-winding
	Capacitance(pF) Primary/Secondary	Capacitance w/o core (pF)
4	3.3/4.3	2.3
5	3.5/4.6	2.5
6	5.1/6.2	4.1

Transformer with both N=6 and N=5 are fabricated for experimental tests. Testing results are tabulated in Table II. The results verified the reduction on inter-winding capacitance for the transformer both with and without the planar core. There is a drop on overall efficiency for N=5 design because with one turn less, peak flux density for the core gets increased, which increases the core loss. Moreover, with just one turn per layer, more vias are used for the layout and the winding loss also increases. To have the minimal inter-winding capacitance design for the transformer while not increasing the core loss significantly, N=5 layout is chosen for the transformer. Final design achieves $<5 \text{ pF}$ coupling capacitance and 4mm on-board height.

The fabricated gate driver board for a single module is shown in Fig.10.

C. Driver Loop Inductance Minimization

Driving loop inductance minimization is another critical aspect for gate driver optimization. High loop inductance can cause severe LCR oscillation in the driving loop that may lead to gate break down, it can also deteriorate shoot-through fault caused by cross-talk of top and bottom switch in a phase leg[17]. To minimize driver loop inductance, self-inductance of forward-path and return-path of both charging and discharging

TABLE II: Achieved performances of the transformer with N=6 and N=5.

		N=6	N=5
Inter-Winding Capacitance(pF)	Bare Board	4.1	2.5
	Board+Core	7.6	4.3
Inductance (μH)	Magnetizing	46	38
	Leakage	1.6	1.6
Max. P_{out} (W)	V_{out} within $\pm 1V$ of 24V	2.65	2.62
Efficiency	88% full load	0.85	0.84
	46% full load	0.82	0.72
Size	Volume	$3cm^3$	$3cm^3$
	On-board Height	4mm	4mm
Operating frequency	440kHz		

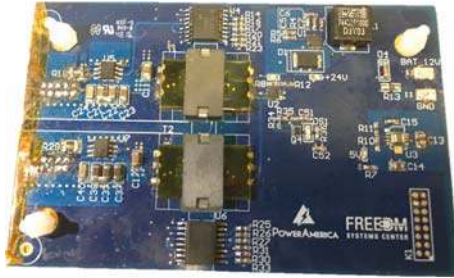


Fig. 10: Hardware picture of the fabricated gate driver for single module.

loop should be minimized, and the mutual-inductance between the paths should be maximized. In [18], a vertical loop concept is proposed and verified for minimal driver loop inductance layout. The method is used in this work, where the forward and return paths are designed on adjacent layers of PCB. The layout of driver loop is shown in Fig.11. ANSYS Q3D simulation results on loop inductance are 2.2nH for charging loop and 1.3nH for discharging loop.

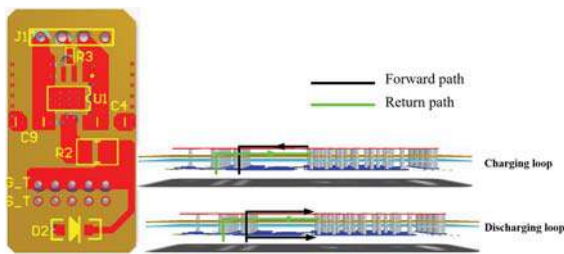


Fig. 11: Layout of the driving loop for charging loop and discharging loop.

The board-to-module connector inductance can actually introduce higher parasitic inductance than from driver loop PCB layout. Therefore, the connector inductance needs to be eliminated. In this work, a split gate driver structure is used, where the driver loop circuit is designed on a 'local driver' that directly connects with the module $G-S$ terminals. The rest part of the gate driver is designed on the 'main driver' board and connects with the 'local driver' vertically. The 'main

driver' board only provides +19V/-5V rails and the PWM signal which is more tolerable to parasitics, the 'main driver' and 'local driver' can be connected with relatively longer connector. The position of 'local driver' and 'main driver' are shown in Fig.12.



Fig. 12: Position of the 'local driver' and 'main driver' to build the split gate driver.

IV. SHUNT BASED CURRENT SENSOR WITH LOW PROFILE AND HIGH CMRR

The designed shunt current sensor circuit is based on TI's isolation amplifier AMC1301[19], which has $\Sigma-\Delta$ modulator for the AD conversion and capacitive barrier for isolation. In a shunt resistor based current sensing structure, the switching node common mode voltage is directly connected to the input of sensor circuit. Therefore, a high common mode rejection ratio (CMRR) is critical to the design of shunt based current sensor. High CMRR can be achieved mainly by two methods. One approach is to use instrumentation amplifier as the front-end since this type of amplifier is designed to have high CMRR over a wide frequency range. Another approach is to make the signal chain as symmetrical as possible. An instrumentation amplifier ISL28633 is used as the front-end interface between shunt resistor and isolation amplifier, the instrumentation amplifier is fully differential in and fully differential out that also achieves symmetrical signal chain for the whole circuit. The designed current measurement range is 200A, shunt resistor loss is 50W if the whole input range (250mV) of AMC1301 is directly used. With instrumentation amplifier, the full input voltage is reduced to 25mV, which makes the design more practical.

Fig.13 shows the testing result of the shunt current sensor. Sinusoidal current of about $150A_{pp}$ is modulated under 1kV DC-link. Fig.13(a) shows the current waveform using commercial current probe. Fig.13(b) shows the DSP sampled data for the same current. The result verifies good noise rejection performance on the designed shunt current sensor. Fig.14 shows the picture of the shunt current sensor, the shunt resistors are designed on the PCB busbar with the voltage signal transmitted to sensor circuit input by twisted wire. The overall design achieves very low profile.

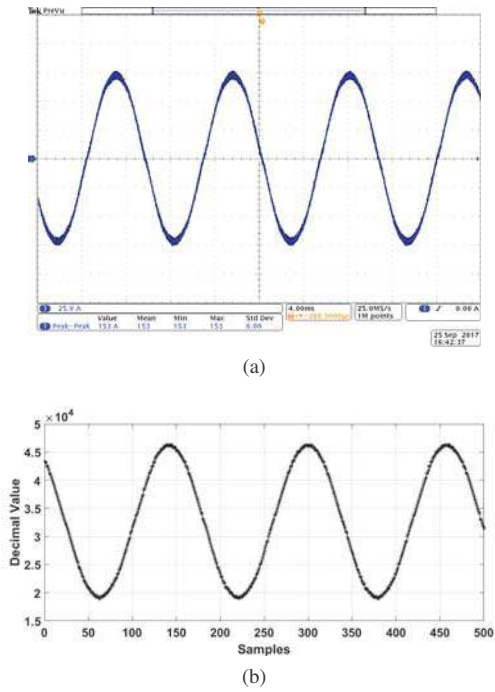


Fig. 13: Testing result of the shunt current sensor (a)output current measured with commercial probe (b)DSP sampled data plotted in MATLAB.



Fig. 14: Hardware picture of the low profile shunt based current sensor.

V. BACK-TO-BACK INVERTER HIGH POWER CIRCULATING TEST METHOD

In this section a new testing strategy on high power traction inverter is discussed. Conventional method of using LR load for inverter testing requires three phase load bank and high power DC supply. To change power factor of inverter output, different fundamental frequency, inductor and resistor values have to be calculated accordingly. The method proposed in this work achieves power circulating between the source inverter and the DUT, therefore large load bank is not needed and only a low power DC supply is used to hold the DC bus. By doing closed-loop current control, power factor can be conveniently changed.

The setup consists of two inverters connected back-to-back with three inductors in between as shown in Fig.15. The setup

can be regarded as a traction inverter driving a three-phase AC motor with back EMF. Therefore, the concept of field oriented control on three phase AC motor can be applied on the power circulating strategy. First, the three phase sinusoidal back EMF voltages E_a , E_b and E_c are synthesized by a rotating space vector E in $\alpha-\beta$ coordinate. The space vector has magnitude E and rotates at fundamental frequency ω . The driving voltage V_a , V_b and V_c can also be denoted by space vector V in $\alpha-\beta$ coordinate. Their differential voltage is applied on the inductor. By placing the two space vectors in the synchronous reference frame of the driving inverter and aligning the back EMF vector E on the d -axis of the synchronous reference frame, the input and output apparent power as well as power factor of the two inverters can be controlled by the phase and magnitude of current vector I . Specifically, if $I_q = 0$, unity power factor operation on the DUT can be achieved. This concept is shown in Fig.16.

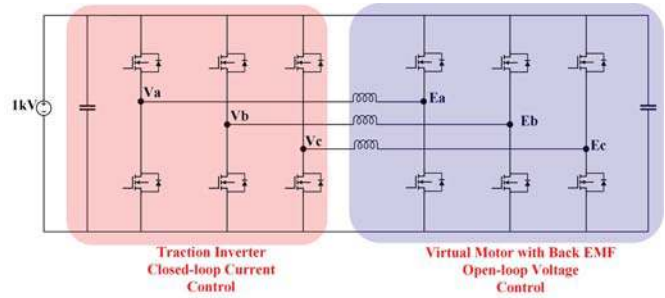


Fig. 15: Hardware setup of the high power circulating test strategy.

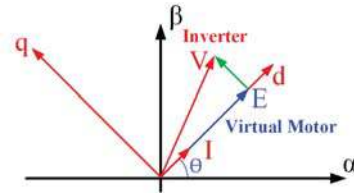


Fig. 16: Demonstration of the circulating strategy in synchronous reference frame.

Using inverse Clarke Transformation, the three phase EMF in stationary coordinate can be obtained as shown in (5), where $\theta = \omega t$. The back EMF are modulated by SPWM in open loop.

$$\begin{bmatrix} E_a \\ E_b \\ E_c \end{bmatrix} = \begin{bmatrix} 1 & 0 \\ -\frac{1}{2} & \frac{\sqrt{3}}{2} \\ -\frac{1}{2} & -\frac{\sqrt{3}}{2} \end{bmatrix} \begin{bmatrix} E \cdot \cos \theta \\ E \cdot \sin \theta \end{bmatrix} \quad (5)$$

The $d-q$ model of the virtual motor in synchronous reference frame can be expressed by (6) where V_d and V_q are the terminal voltages, E_d and E_q are the back EMF voltages in $d-q$ frame. The current controller can be designed based on the model as shown in Fig.17. The V_d and V_q are generated

by PI regulators with compensation terms. A zero-sequence current suppressor is also added to the controller to mitigate the zero-sequence current issue inherent to the back-to-back inverter setup[20]-[22].

$$\begin{aligned} V_d &= L \frac{di_d}{dt} + \omega L i_q + E_d \\ V_q &= L \frac{di_q}{dt} - \omega L i_d + E_q \end{aligned} \quad (6)$$

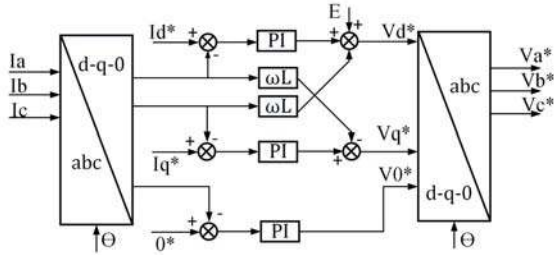


Fig. 17: Block diagram of the current controller.

For practical implementation, two types of synchronization need to be implemented. As the d axis of the synchronous reference frame need to be aligned with the back EMF vector E , the rotation angle θ used for both controllers must be well synchronized. Failing to do so will cause steady state error on the output. Moreover, the PWM carriers of both controllers need to be synchronized to reduce the ripple current on the load inductors and system loss[23]. An external synchronization controller generates square wave signal at fundamental frequency to synchronize both the transformation angle and PWM carrier. Hardware implementation for the synchronization and experimental results on zero sequence current reduction are elaborated in[24].

The 100kW full continuous power operation of the SiC inverter is tested by the back-to-back circulating method as shown in Fig.18. The inverter is operated under 1kV DC-link, 160A_{pk} phase current and 30kHz switching frequency. Fig.18(a) shows the three phase sinusoidal waveform, Fig.18(b) shows the DC-link current waveform with mean value of 100A, and the V_{ds} waveform with an overshoot of 18% maximum. With the back-to-back circulating test strategy, the 1kV DC power supply only needs to provide around 5kW output to the whole system, which is the total loss generated by the system. The results also verifies the performance of the designed shunt based current sensor working under 100kW condition.

VI. CONCLUSION

This paper discusses the design on a 100kW SiC traction inverter with 1kV DC-link. To achieve low profile, planar structure is adopted. The optimizations on the PCB busbar helps to achieve low characteristic impedance, symmetrical commutation loop and low loop inductance that is critical to reduce the V_{ds} overshoot. The planar transformer significantly reduces overall height of the gate driver, and by optimizing the

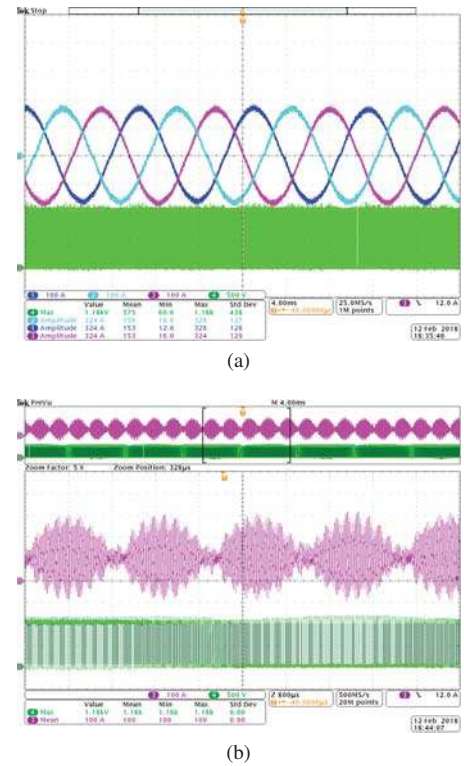


Fig. 18: (a)Three-phase current waveform of the SiC inverter;(b)DC-link current waveform with mean value of 100A and V_{ds} waveform with overshoot of 18% max.

winding layout, low isolation capacitance is achieved. Shunt resistor based switching node current sensor is designed for the high power traction inverter, the design is a low profile low cost solution, which achieves high common mode noise rejection, and has been verified by a closed-loop current control up to 100kW. The proposed back-to-back inverters high power circulating test strategy eliminates the need on high power load bank and power supply, and is capable of varying power level as well as power factor of the DUT up to 100kW level.

ACKNOWLEDGMENT

The information, data, or work presented herein was funded in part by the Office of Energy Efficiency and Renewable Energy (EERE), U.S. Department of Energy, under Award Number DE-EE0006521 with the North Carolina State University, PowerAmerica Institute. This work made use of FREEDM ERC shared facilities supported by NSF under award no. EEC-0812121.

DISCLAIMER

The information, data, or work presented herein was funded in part by an agency of the United States Government. Neither the United States Government nor any agency thereof, nor any of their employees, makes any warranty, express or implied, or assumes any legal liability or responsibility for the accuracy,

completeness, or usefulness of any information, apparatus, product, or process disclosed, or represents that its use would not infringe privately owned rights. Reference herein to any specific commercial product, process, or service by trade name, trademark, manufacturer, or otherwise does not necessarily constitute or imply its endorsement, recommendation, or favoring by the United States Government or any agency thereof. The views and opinions of authors expressed herein do not necessarily state or reflect those of the United States Government or any agency thereof.

REFERENCES

- [1] K. Yamaguchi, K. Katsura and T. Yamada, "Comprehensive evaluation and design of SiC-Based high power density inverter, 70kW/liter, 50kW/kg", 2016 IEEE 8th International Power Electronics and Motion Control Conference (IPEMC-ECCE Asia), Hefei, 2016, pp. 1-7.
- [2] T. J. Han, J. Nagashima, S. J. Kim, S. Kulkarni, and F. Barlow, "High density 50 kW SiC inverter systems using a JFET based six-pack power module", Proc. IEEE Int. Conf. Power Electron. ECCE-Asia, May 2011, pp. 764769.
- [3] S. Yin, K. J. Tseng, R. Simanjorang, Y. Liu and J. Pou, "A 50-kW High-Frequency and High-Efficiency SiC Voltage Source Inverter for More Electric Aircraft", IEEE Transactions on Industrial Electronics, vol. 64, no. 11, pp. 9124-9134, Nov. 2017.
- [4] D. Rahman et al., "Design methodology for a planarized high power density EV/HEV traction drive using SiC power modules", 2016 IEEE Energy Conversion Congress and Exposition (ECCE), Milwaukee, WI, 2016, pp. 1-7.
- [5] "60 kW SiC-Inverter for High-Speed Drives", https://www.mikroelektronik.fraunhofer.de/content/dam/mikroelektronik/Datenbltter/IIS_60kW_DB.pdf
- [6] S. Yano et al., "Development of compact power control unit for HEVs", 2017 IEEE Energy Conversion Congress and Exposition (ECCE), Cincinnati, OH, 2017, pp. 584-588.
- [7] A. H. Wijenayake et al., "Design of a 250 kW, 1200 V SiC MOSFET-based three-phase inverter by considering a subsystem level design optimization approach", 2017 IEEE Energy Conversion Congress and Exposition (ECCE), Cincinnati, OH, 2017, pp. 939-946.
- [8] C. Jung, "Power Up with 800-V Systems: The benefits of upgrading voltage power for battery electric passenger vehicles", IEEE Electrification Magazine, vol. 5, no. 1, pp. 53-58, March 2017.
- [9] Volker Reber, "New Possibilities with 800-Volt Charging", Porsche Engineering Magazine, Issue1/2016.
- [10] J. W. Kolar and S. D. Round, "Analytical calculation of the RMS current stress on the DC-link capacitor of voltage-PWM converter systems", IEEE Proceedings - Electric Power Applications, vol. 153, no. 4, pp. 535-543, July 2006.
- [11] B. Aberg, R. S. K. Moorthy, L. Yang, W. Yu and I. Husain, "Estimation and minimization of power loop inductance in 135 kW SiC traction inverter", 2018 IEEE Applied Power Electronics Conference and Exposition (APEC), San Antonio, TX, USA, 2018, pp.1772-1777.
- [12] N. R. Mehrabadi, I. Cvetkovic, J. Wang, R. Burgos and D. Boroyevich, "Busbar design for SiC-based H-bridge PEBB using 1.7 kV, 400 A SiC MOSFETs operating at 100 kHz", 2016 IEEE Energy Conversion Congress and Exposition (ECCE), Milwaukee, WI, 2016, pp. 1-7.
- [13] D. O. Thomas, M. Sylvain, G. J. Michel, J. L. Schanen, and A. Perre-gaux, "Reduction of conducted EMC using busbar stray elements", Proc. 24th Annu. IEEE Appl. Power Electron. Conf. Expo., 2009, pp. 2028 - 2033.
- [14] Rui Gao, Li Yang, Wensong Yu, Iqbal Husain, "Single Chip Enabled High Frequency Link Based Isolated Bias Supply for Silicon Carbide MOSFET Six-Pack Power Module Gate Drivers", 2016 IEEE Energy Conversion Congress and Exposition (ECCE), Milwaukee, WI.
- [15] M. Mu and F. C. Lee, "A new core loss model for rectangular AC voltages", 2014 IEEE Energy Conversion Congress and Exposition (ECCE), Pittsburgh, PA, 2014, pp. 5214-5220.
- [16] B. Sun, R. Burgos and D. Boroyevich, "2 W Gate drive power supply design with PCB-embedded transformer substrate", 2017 IEEE Applied Power Electronics Conference and Exposition (APEC), Tampa, FL, 2017, pp. 197-204.
- [17] Z. Zhang, F. Wang, L. M. Tolbert and B. J. Blalock, "Active Gate Driver for Crosstalk Suppression of SiC Devices in a Phase-Leg Configuration", IEEE Transactions on Power Electronics, vol. 29, no. 4, pp. 1986-1997, April 2014.
- [18] D. Reusch and J. Strydom, "Understanding the Effect of PCB Layout on Circuit Performance in a High-Frequency Gallium-Nitride-Based Point of Load Converter", IEEE Transactions on Power Electronics, vol. 29, no. 4, pp. 2008-2015, April 2014.
- [19] TI Designs (TIDA-00445), "Shunt-Based, 200-A Peak Current Measurement Reference Design Using Reinforced Isolation Amplifier".
- [20] J. Korhonen, J. Honkanen, T. J. Krkkinen, J. Nerg and P. Silventoinen, "Modulation and control methods to reduce zero sequence current in open-end winding motors", 2017 IEEE International Electric Machines and Drives Conference (IEMDC), Miami, FL, 2017, pp. 1-6.
- [21] H. Zhan, Z. Q. Zhu and M. Odavic, "Analysis and Suppression of Zero Sequence Circulating Current in Open Winding PMSM Drives with Common DC Bus", IEEE Transactions on Industry Applications, vol. 53, no. 4, pp. 3609-3620, July-Aug. 2017.
- [22] Q. An, J. Liu, Z. Peng, L. Sun and L. Sun, "Dual-Space Vector Control of Open-End Winding Permanent Magnet Synchronous Motor Drive Fed by Dual Inverter", IEEE Transactions on Power Electronics, vol. 31, no. 12, pp. 8329-8342, Dec. 2016.
- [23] L.G. Gonzalez, G. Garcer, E. Figueres, R. Gonzalez, "Effects of the PWM carrier signals synchronization on the DC-link current in back-to-back converters", Applied Energy, Volume 87, Issue 8, 2010, Pages 2491-2499.
- [24] Yukun Luo, Li Yang, Wensong Yu, Iqbal Husain, "A Variable Power Factor High Power Testbed for Traction Inverter with Back-to-Back Converters", 2018 IEEE Energy Conversion Congress and Exposition (ECCE), Portland, OR, 2018.